



UWS Academic Portal

Lateral resistance performance evaluation of cold-formed steel zero-tolerance bolted moment-resisting frames

Wrzesien, Andrzej; McCrum, Daniel P.; Mishra, Sohini; Broderick, Brian M.; Lim, James B.P.

Published in:
Structures

DOI:
[10.1016/j.istruc.2023.02.051](https://doi.org/10.1016/j.istruc.2023.02.051)

E-pub ahead of print: 30/04/2023

Document Version
Publisher's PDF, also known as Version of record

[Link to publication on the UWS Academic Portal](#)

Citation for published version (APA):

Wrzesien, A., McCrum, D. P., Mishra, S., Broderick, B. M., & Lim, J. B. P. (2023). Lateral resistance performance evaluation of cold-formed steel zero-tolerance bolted moment-resisting frames. *Structures*, *50*, 590-602. <https://doi.org/10.1016/j.istruc.2023.02.051>

General rights

Copyright and moral rights for the publications made accessible in the UWS Academic Portal are retained by the authors and/or other copyright owners and it is a condition of accessing publications that users recognise and abide by the legal requirements associated with these rights.

Take down policy

If you believe that this document breaches copyright please contact pure@uws.ac.uk providing details, and we will remove access to the work immediately and investigate your claim.



Lateral resistance performance evaluation of cold-formed steel zero-tolerance bolted moment-resisting frames

Andrzej Wrzesien^a, Daniel P. McCrum^{b,*}, Sohini Mishra^b, Brian M. Broderick^c, James B.P. Lim^{d,e}

^a School of Computing, Engineering and Physical Sciences, University of the West Scotland, United Kingdom

^b School of Civil Engineering, University College Dublin, Newstead Building, Dublin 4, Ireland

^c Department of Civil, Structural & Environmental Engineering, Trinity College Dublin, Ireland

^d School of Engineering, University of Waikato, Hamilton, New Zealand

^e Department of Civil and Environmental Engineering, The University of Auckland, New Zealand

ARTICLE INFO

Keywords:

Cold-formed steel
Moment-resisting frame
Monotonic testing
Zero-tolerance bolted connections
Monosymmetric section

ABSTRACT

The experimental and analytical lateral load resisting behaviour of three cold-formed steel (CFS) moment-resisting frames with zero-tolerance bolted joints were investigated to understand the potential application of such joints in medium-span CFS portal frames. Strain gauge data were used to measure total longitudinal stresses in the column sections and were compared with analytical models. It was found that the bi-moment stress component was the second largest component after major-axis bending and can be analytically and conservatively estimated. The validity of the design approaches of monosymmetric and doubly symmetric back-to-back channel columns were also investigated. For the first time, the potential application of zero-tolerance jointed frames in medium-span CFS portal frames is demonstrated and conservative analysis and design approaches (monosymmetric) are employed.

1. Introduction

Portal frame buildings are one of the most popular and efficient types of steel structures accounting for 90 % of all single storey buildings and 50 % of all the construction steel used in the UK each year [1]. Traditionally, the primary structure of portal frames (moment-resisting) employs hot-rolled steel sections. Cold-formed steel (CFS) members were typically only used for constructing the building envelope e.g., sheeting and purlins. In recent decades, extensive research in the field of CFS structures led to the development of several types of built-up sections, e.g., face-to-face, back-to-back gapped CFS sections, etc. [2–5] with increased axial and lateral load-resisting capacity, that are a viable alternative to conventional hot-rolled steel sections for modest span frames (typical spans around 10–12 m [6]).

Several previous studies have demonstrated the viability of using CFS sections to construct portal frames of modest spans ([7–10]). The key feature of these studies was that eaves and apex joints were designed to function as rigid connections. Such joints, however, were either expensive to manufacture or physically difficult to erect on site [11]. Lim and Nethercot [12–14] and Chung and Yu [15] experimentally

determined the rotational stiffness of bolted moment-resisting CFS portal frame joints and subsequently applied the measured rotational stiffness to frame analysis and design. In both studies, the bolted moment-resisting connections, for the eaves and apex joints, were formed using brackets, to ensure that they were practical to manufacture and assemble on site. More recently, [16] conducted extensive numerical studies on this form of joint and used the results to develop formulae to predict the strength of such CFS brackets. Several researchers have also concentrated on increasing the rotational stiffness of the eaves and apex joints ([17–21]), which is beneficial for the overall lateral response of the bare frame, in terms of reducing frame serviceability deflections, but significantly increases the cost [22]. CFS joints with high rotational stiffness or full-strength moment-resistance often require welded hot-rolled steel brackets e.g. [23]. Typical CFS bolted moment-resisting frames employ bolts placed in holes, with diameters 2 mm larger than the bolt diameter, to ensure the required construction tolerance. When oversized holes are used, the rotational stiffness of the joint is different during the slip and bearing stages of response, with the joint acting as a pin until the post-slip stage is reached. This joint stiffness characteristic can lead to excessive lateral frame deflections under wind and

* Corresponding author.

E-mail address: daniel.mccrum@ucd.ie (D.P. McCrum).

<https://doi.org/10.1016/j.istruc.2023.02.051>

Received 8 June 2022; Received in revised form 15 December 2022; Accepted 9 February 2023

Available online 20 February 2023

2352-0124/© 2023 The Authors. Published by Elsevier Ltd on behalf of Institution of Structural Engineers. This is an open access article under the CC BY license (<http://creativecommons.org/licenses/by/4.0/>).

earthquake loading, which in turn may result in greater load transfer between frames via external sheeting (stressed skin action) [22,24,25].

Bolt slip in oversized holes can occur during frame erection and may result in changes in the slope of the rafters or the verticality of the columns, presenting further alignment problems. To prevent sagging or misalignment due to bolt slip, frame erectors often use self-drilling, self-tapping screws (also known as tek screws) in conjunction with standard bolts. Such ‘mixed fastener’ connections were investigated by Pouladi et al. [26]. They demonstrated that the strength and stiffness of the joints were controlled by the tek screws alone, and that shearing of the screws was observed at the ultimate state. A tek screw connection was investigated by Mills et al. [10] but due to the relatively small shear capacity of the standard tek screws, such joints are only practical for short-spanning frames. Tek screws can also fail in shear rather than bearing causing very sudden failure and decreasing the ductility of the connection. They are therefore not used in the portal frame construction of medium and large spans.

The aim of this study is to investigate the lateral load resisting capacity of CFS bolted moment-resisting frames using zero-tolerance bolts (i.e. similar conceptual performance to tek screws in terms of zero-slip) to form the joints and also investigate such frames without hot-rolled steel brackets. There is a lack of analytical and experimental results on the effect of the bi-moment on the overall longitudinal stress distribution in CFS column sections, which is addressed in this paper. The normative guidance on the design of CFS portal frames joint needs to be also improved. Lim et al., [27,28] reported that back-to-back channel sections should not be designed as compound doubly symmetric beams as they can act individually around the connection point, thus behaving as monosymmetric elements. Concurrently, Mojtabei et al., [29,30] used experimental results published by Lim and Nethercot [12,13] to produce an extensive numerical study and proposed a resistance reduction factor for 2x2, 3x3, 4x4 bolted connections. Others [31,32] have also acknowledged that, for monosymmetric sections subjected to lateral torsional buckling, Eurocode 3 [33,34] provides no specific rules for the calculation of the elastic critical moment due to the asymmetry of the section. In this paper, therefore, the cross-sectional resistance of the compression side columns of portal frames subjected to combined axial compression and bending moment has been investigated experimentally and compared with analytical results, considering both the doubly symmetric (recommended by [35]) and monosymmetric conditions.

2. Portal frame joint stiffness

The lateral load-resisting response of three CFS portal frames was investigated. Three test frames with different sizes of back-to-back channel section members representing low (C20018), medium (C25020) and high strength frames (C30025) were examined. Fig. 1 shows the C25020 frame. All test frames employed moment-resisting zero-tolerance eaves connections as described in the following section. Then full-scale frame stiffness was established through testing and the numerical models were validated.

An early contribution to knowledge on the behaviour of bolted moment connections was the work produced by Zadanfarrokh [36]. Zaharia and Dubina [37] also conducted an experimental study on the flexibility of a single fixing lap joint similar to that reported by Zadanfarrokh and Bryan [36]. It was also demonstrated by the above research, that by using the principles of the elastic load distribution, the stiffness of the bolt group can be analytically derived and successfully modelled employing linear and rotational springs. Concurrently, Dubina [38], Wuwer et al., [39], and Bućmys et al. [40], presented the possibility of using codified methods for calculating the shear stiffness of each joint component (component method specific to hot-rolled steel joints according to [41]) in predicting axial and rotational stiffness of joints. It should be highlighted that the above research investigated mixed joints consisting of CFS and hot-rolled steel plates. The principles of the elastic design method for the load distribution between the bolts were employed and this model has shown good accuracy in predicting joint stiffness. More recently, Wrzesien et al. [42] investigated the rotational stiffness of the moment-resisting joints and the applicability of the elastic model in predicting a joint’s rotational stiffness was also confirmed in the aforementioned study.

2.1. Connection details

In the zero-tolerance joints, the pre-punched channel sections were used as drilling templates to cut 18 mm dia. holes in the brackets using a multi-tooth annular cutter. Standard fully threaded M18 × 40, 8.8 Grade, Bright Zinc Plated (BZP) bolts to BS EN ISO 4017:2014 [45], with washers on both sides, were used. Three back-to-back channel sections were employed for the column and rafter members classified as C20018, C25020 and C30025 with the cross-sectional bending moment-

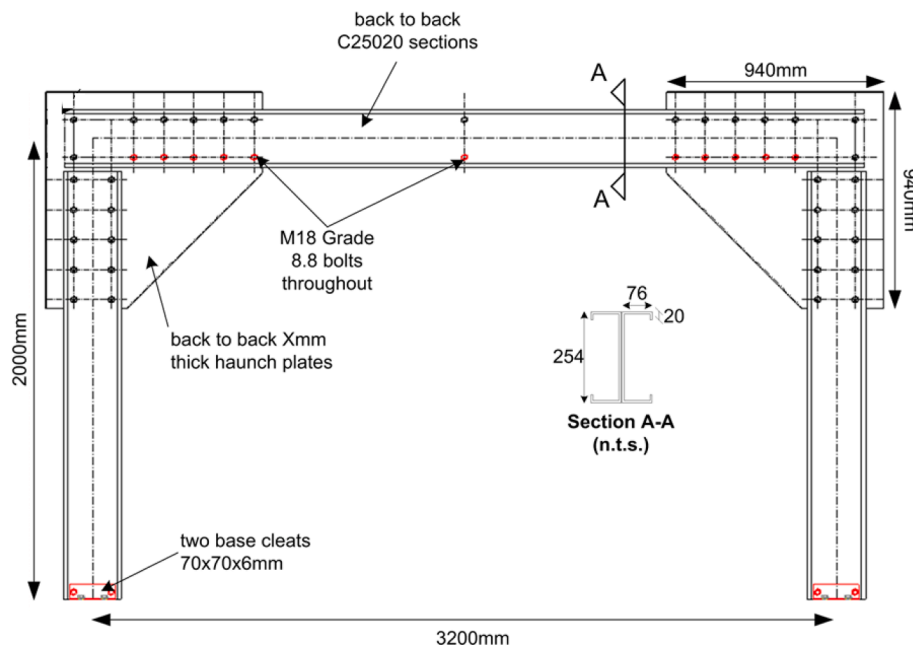


Fig. 1. Typical cold-formed steel portal frame considered in this study [43,44].

resistances ranging from 28.2 to 75.0 kNm (calculated using [33]). All the eaves connection brackets were made by press-breaking from 3 mm thick galvanized steel plates (S450GD + Z275 steel grade to BS EN 10346: 2015 [46]), with folded stiffeners to protect against local buckling under both ‘closing’ and ‘opening’ moments. All the brackets were folded with a 2.75 mm bend radius. The eaves joint dimensions for each cross-section size are presented in Fig. 2.

2.2. Column/rafter members and base connections

In each test, back-to-back channel sections were used for columns and rafters. Sections were manufactured from S450GD + Z275 grade steel according to BS EN 10346:2015 [46]. The connection brackets (C200A, C250A and C300A) were manufactured from steel plates of 3 mm thickness and the same grade of steel as the sections. For the base connections (refer to Figs. 1 and 2), an industry-standard angle

connection detail was used. For the frame of the lowest capacity (C20018), CFS base cleat angles were used and manufactured from the same steel as the brackets. Base cleats for C25020 and C30025 were manufactured from mild steel flat bars (S275JR) of 6 mm thickness. Dimensions of channels and base cleats are given in Table 1.

2.3. Tensile coupon tests

In total, 12 tensile tests were carried out to determine the mechanical properties of all steel gauges used for each of the test components. The tensile coupons were cut out of steel channels and tested according to BS EN 10002-1:2001 [47] using 20 mm wide coupons. Coupons were tested in an Instron universal testing machine using friction grips. A non-contact Advanced Video Extensometer (AVE 2663-821) with a 10 mm gauge length was used to measure the longitudinal strain. Three coupons for each steel gauge (1.8, 2.0, 2.5 & 3.0 mm) were tested to obtain the

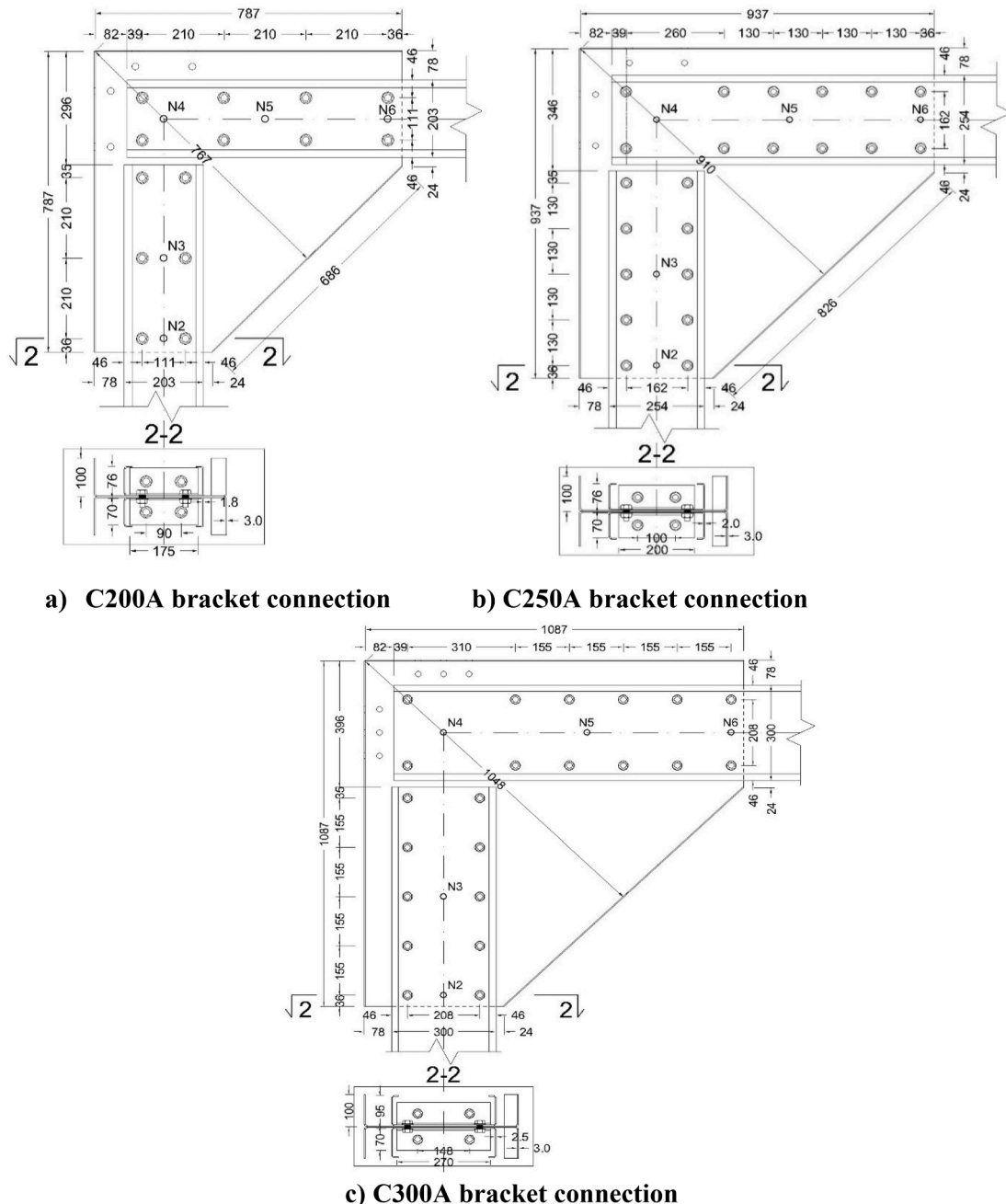
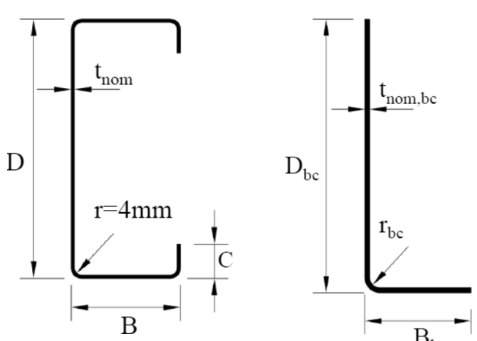


Fig. 2. Eaves connection details [43].

Table 1
Channel section and base cleat geometries.



Test frame	Nominal dimensions (mm)							
	Section				Base cleat			
	D	B	C	t _{nom}	D _{bc}	B _{bc}	r _{bc}	t _{nom, bc}
C20018	203.0	76.0	20.0	1.80	70.0	70.0	2.75	3.00
C25020	254.0	76.0	20.0	2.00	70.0	70.0	9.0	6.00
C30025	300.0	95.0	20.0	2.50	70.0	70.0	9.0	6.00

average value. A summary of mechanical properties relevant to CFS is presented in Table 2.

2.4. Details of the finite element modelling of the eaves bracket

2.4.1. Geometry and material models for brackets

The FEA program ABAQUS (2018) [48] was used to develop a numerical model to predict the equivalent flexural stiffness of the tapered eaves bracket. The aim was to numerically establish in-plane deformation of the bracket at points coinciding with Centres of Rotations (COR). The locations of these points for the column and rafter bolt groups are denoted N3 and N5 and can be seen in Fig. 3. The flexural stiffnesses of the column and rafter parts of the bracket, established through FEA, were expressed as equivalent beams with the finite lengths (l_{3-4} , l_{4-5}) and equivalent second moments of area (I_{3-4} , I_{4-5}).

The equivalent second moments of area were calculated from the formulae:

$$I_{i-j} = \frac{F_i l_{i-j}^3}{3E\delta_i} \text{ where;}$$

F_i – Total load applied to the bracket and causing the displacement δ_i

l_{i-j} – Finite length of the bracket (see Fig. 3a)

E – Young’s Modulus

δ_i – Displacement of the Center of Gravity for respective bolt group

The nominal cross-section dimensions were modelled as presented in Fig. 2. The elastic perfectly plastic stress–strain relationship was applied to model steel brackets using the following mechanical properties: Young’s Modules, $E = 210$ GPa, Poisson’s Ration, $\nu = 0.3$ and Proof

Table 2
Steel properties obtained from tensile coupon tests.

Component	Position	Number of tests	Proof strength $R_{p,0.2}$ (MPa)	Tensile strength R_m (MPa)	Non-proportional elongation at max. stress $A_{g,t}$ (%)	Elongation after fracture A_t (%)
C20018	Web	3	457 (SD = 29)	543 (SD = 2)	13	19
C25020	Web	3	482 (SD = 12)	596 (SD = 2)	13	19
C30025	Web	3	475 (SD = 5)	573 (SD = 5)	12	19
Brackets C200A, C250A & C300A	Web	3	489 (SD = 2)	546 (SD = 2)	12	19

Stress, $R_{p,0.2} = 489$ MPa.

2.4.2. Element type and mesh size

S4R shell elements were used to model the CFS bracket, as the S4R elements are linear 4-noded quadrilateral thick shell elements that have six degrees of freedom per node. No geometric imperfections [49–51] were considered, as only estimates of the flexural stiffness of the bracket are needed as these stiffnesses will later be expressed as an equivalent stiffness of a beam element. The mesh sensitivity analysis was conducted, and the results suggested that a mesh size of 20×20 mm (length by width) was suitable for the CFS bracket. The bracket was partitioned so the key nodes are represented and a more structured mesh can be applied. A finer mesh size was also used near the rounded corners (Fig. 3 (b)).

2.4.3. Boundary conditions and loading procedure

To establish the flexural stiffness of the bracket and express it as an equivalent beam element of a finite length, the edge representing the line of symmetry was restrained against translation in all 3 directions (see Fig. 3(c)). This line is passing through node N4 (see Fig. 3(a)) where the equivalent beams representing the column and rafter part of the bracket will join (see Fig. 3(c)). The loading was applied via a pair of equal forces applied through the locations of two bolts located on the lines passing through Centres of Rotations (N3 and N5). The displacements of nodes N3 and N5 in the load directions were measured at the maximum load applied.

2.4.4. Bracket flexural stiffness based on the FEA results

It should be noted that linear load–displacement relationships were plotted for brackets under the maximum in-plane bending moments. The failure loads were not investigated as brackets were designed to resist much higher loads than columns/rafters members. The equivalent in-plane flexural stiffnesses of back-to-back eaves brackets are presented in Table 3. The results from Table 3 were applied to the beam analysis model of the entire portal frame to replicate the flexural stiffness of the brackets. Although the FEA shell simulations are commonly used in CFS research, such computational tools are rarely available in structural design practice where beam models are still predominately used. In this paper, a simplified modelling technique is presented which reduces the computational time and effort but also generates an output (see Table 3), that can be easily applied in practice.

3. Portal frame lateral stiffness

The following section presents the analytical evaluation of the frame lateral stiffness which was later used to obtain the analytical load–displacement curve for each test frame. A comparison of the analytical and experimental curves is also presented herein.

3.1. Analytical prediction of frame stiffness

The non-linear elastic frame analysis program Robot Structural

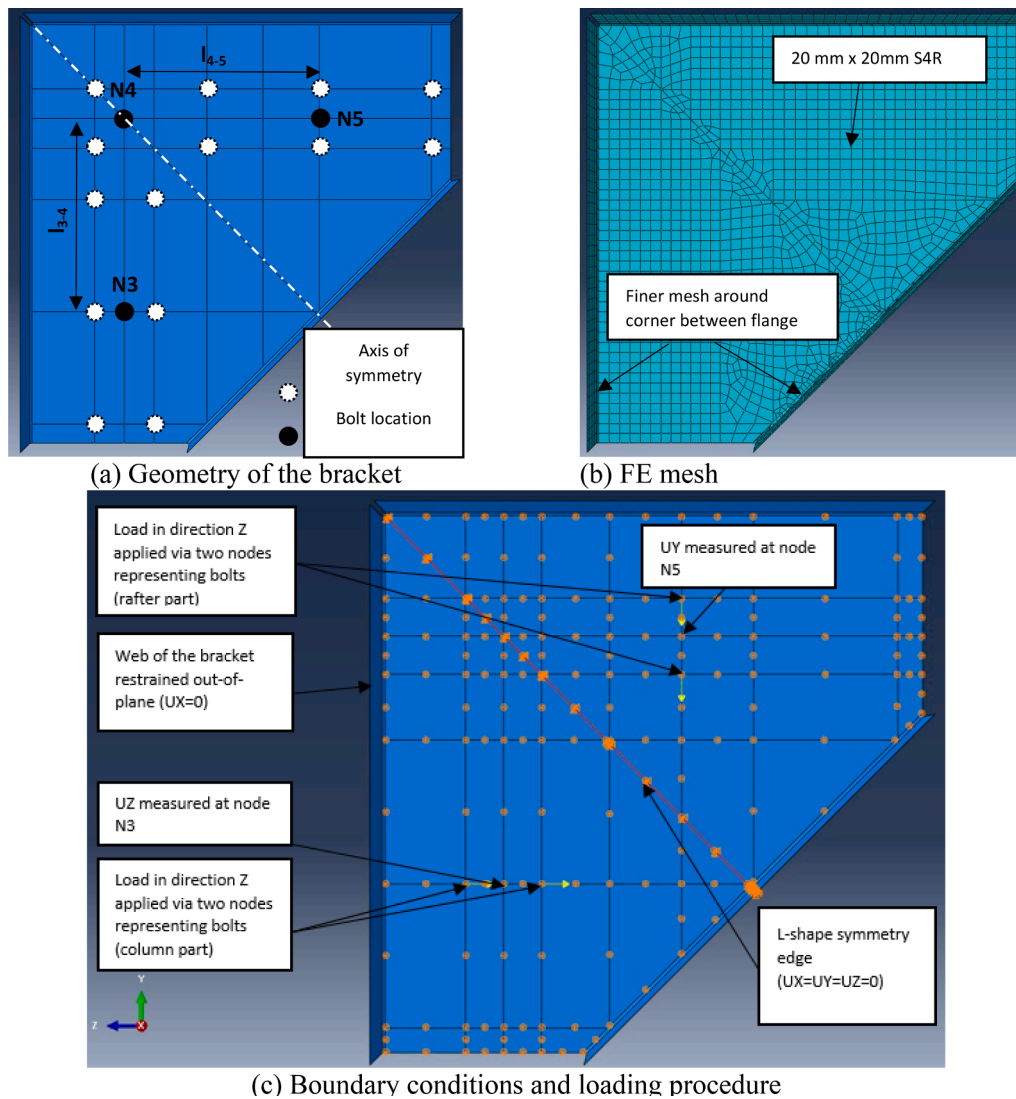


Fig. 3. FE model of the eaves bracket.

Table 3
Beam idealisation of 3D eaves brackets using FEA.

Bracket type	Finite length of the bracket - column l_{3-4} (mm)	Finite length of the bracket - rafter l_{4-5} (mm)	Equivalent second moment of area – column I_{3-4} (mm ⁴)	Equivalent second moment of area – rafter I_{4-5} (mm ⁴)
C200A	365	260	105,193,793	56,977,201
C250A	440	352	159,220,100	105,787,670
C300A	516	413	252,411,138	168,959,559

Analysis Professional 2010 [52] was used to model the lateral load-resisting behaviour of the tested frames. A simple two-dimensional beam idealisation using industry standard design software [43] was chosen and key input data for the rotational stiffness of the zero-tolerance joints are presented in Table 4.

The cross-section area (A) and major axis second moment of area (I_y) were calculated for columns and rafters based on the channel geometries given in Table 4. In the practical design of portal frames, the flexural stiffness of brackets is often assumed the same as the stiffness of the members [35] as this conservatively overestimates flexibility. Such an assumption is not justifiable in this research because in the case of the largest joint C300A, the finite length of the bracket is approximately a

quarter of the column height. Hence, in this paper, a more exact method is employed to establish the flexural stiffness of the brackets as described in Section 2.4. Load-displacement curves obtained from this FEA results were used to represent the flexural stiffness of the bracket as an equivalent prismatic beam (see Table 3).

All key parameters used in the beam idealisation of the tested joint are listed in Table 4 and they include: bolt groups lengths (a_{bg}) and widths (b_{bg}), x- and y-coordinates of the Centres of Rotations, analytical shear stiffness (k_b) and joint rotational stiffness in the bolt-bearing stage (S_j). Joint rotational stiffness was calculated based on the Elastic Theory and two analytical methods for calculating the shear stiffness of a single bolt, bearing into a steel plate (Eurocode 3 [41], and Zadanfarrokh and Bryan [36]) which tend to represent upper and lower bounds of joint rotational stiffness. The bolt group rotational stiffness of the zero-tolerance joint identified from this FEA can be represented as a linear rotational spring for global frame analysis (see Table 4 for the input values).

3.2. Validation experiments

The experimental setup consisted of a CFS portal frame sandwiched between two back-to-back ‘strong reaction frames’ as shown in Fig. 4. Support beams spanned between the two reaction frames as shown in Fig. 4(b). The test frame was then supported off these beams using

Table 4
Parameters used in beam idealisation for tested bolt groups [25]

Test ID.	Bolt array	a_{bg} (mm)	b_{bg} (mm)	x_{cor} (mm)	y_{cor} (mm)	k_b (kN/mm)	S_j (kNm/rad)	Joint Type
C20018	3x2	420	111	210.0	55.5	22.340*	4354	Column
	4x2	630	111	315.0	55.5	22.340*	10,402	Rafter
	3x2	420	111	210.0	55.5	11.613**	2264	Column
	4x2	630	111	315.0	55.5	11.613**	5407	Rafter
C25020	5x2	520	162	260.0	81.0	24.906*	10,052	Column
	6x2	780	162	433.3	81.0	24.906*	21,604	Rafter
	5x2	520	162	260.0	81.0	12.632**	5098	Column
	6x2	780	162	433.3	81.0	12.632**	10,957	Rafter
C30025	5x2	620	208	310.0	104.0	27.305*	16,073	Column
	6x2	930	208	516.7	104.0	27.305*	34,157	Rafter
	5x2	620	208	310.0	104.0	15.000**	8830	Column
	6x2	930	208	516.7	104.0	15.000**	18,764	Rafter

* Shear stiffness of single-bolt lapped joint (k_b) calculated according to [38,39,41]

** Shear stiffness of single-bolt lapped joint (k_b) calculated according to [36]

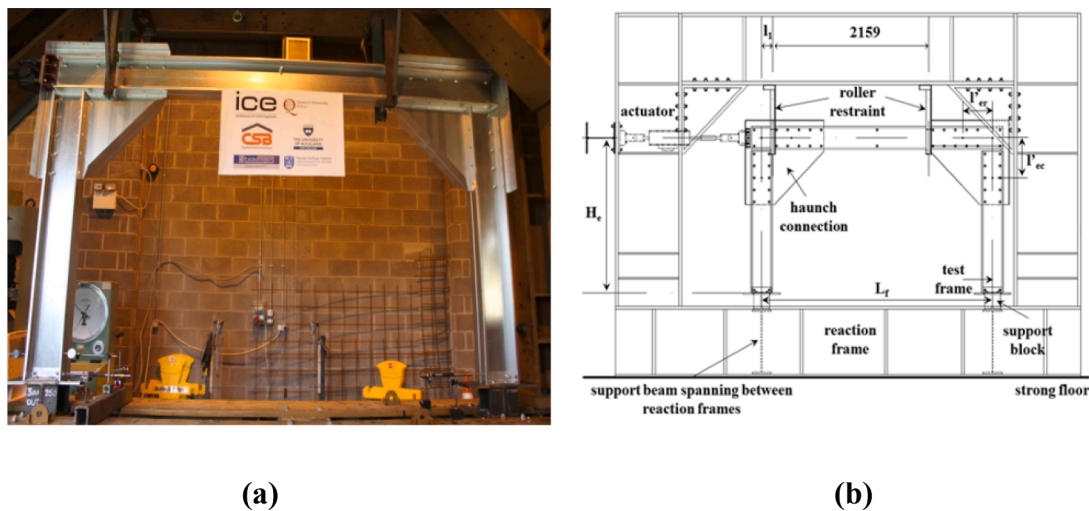


Fig. 4. Test set-up; (a) photograph of C25020 frame prior to test; and (b) schematic drawing of the key dimensions.

fabricated support blocks designed to release bending moments and therefore replicate pinned connections. The actuator was mounted in between the two reaction frames as can be seen in Fig. 4(a) & (b). The

linear hydraulic actuator had a capacity of 150 kN with a stroke of ± 125 mm. The actuator employed an internal load cell and linear variable differential transformer (LVDT) to measure force and

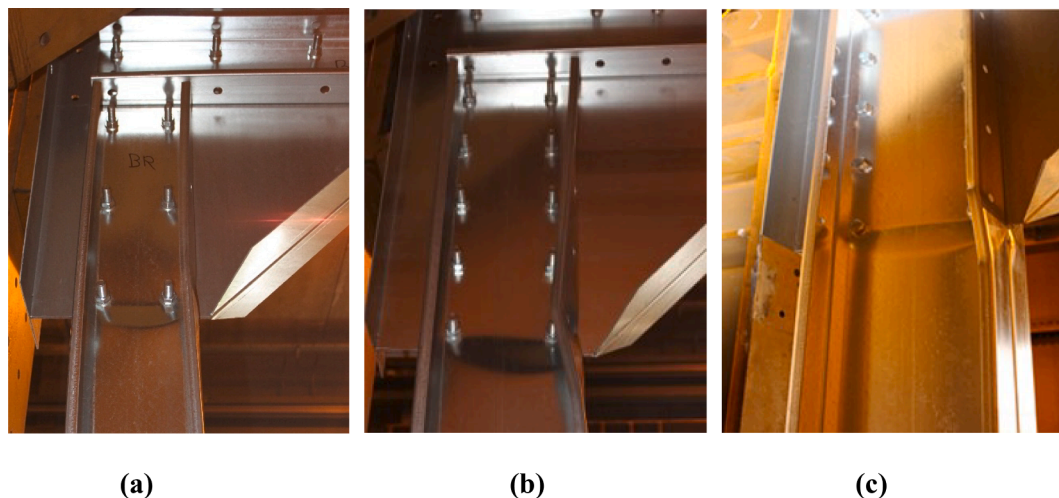


Fig. 5. Failure modes of columns in compression: (a) C20018; (b) C25020; and (c) C30025.

displacement, respectively. In order to prevent out-of-plane displacement of the CFS test frame during the experiments, two roller guides held the test frame in place while allowing the test structure to move ‘frictionless’ in-plan. The geometry of the test set-up with key dimensions is presented in Fig. 4(b). All the tested frames were approximately of 3.2 m span (L_f) and 2.0 m in height (H_e). For each bolt group, the Centre of Rotation (CoR) coinciding with the bolt group centre of gravity was calculated and its location is defined as a Finite Length of the Joint (l'_e) in Fig. 4(b). Every connection bolt was tightened with a torque wrench to the value of 90Nm (equivalent to the torque generated in practice by a typical hand spanner according to [53]). Three monotonic tests were performed, one on each frame.

3.3. Experimental observations

Visual observation of the test frames after each test revealed, local buckling failure of the web, flanges and the web-to-flange junction of the column adjacent to the haunch connection (see Fig. 5). This failure mechanism is attributed to the combined action of bending moment and bi-moment generated in the channel sections around their longitudinal axis of symmetry and in the direction away from the bracket plates.

No shear and bearing damaged was observed at the eaves connections. The peak lateral load recorded for the C20018 (low strength), C25020 (medium strength) and C30025 (high strength) frames were 31.6 kN, 57.6 kN and 105.3 kN, respectively. The experimental load–displacement plots as shown in Fig. 6 clearly indicates the peak lateral loads for the three test frames. It can be seen from the lateral load response in Fig. 6 that the zero-tolerance bolted connections deliver an almost linear load–displacement relationship in the initial stage of loading (working loads) as any loss of lateral stiffness due to slip of bolts in tolerance holes is eliminated. There is also a clear correlation between the thicknesses of the bolted plates, the rotational stiffness of the joint and the overall lateral stiffness of the frame.

3.4. Comparison of experimental and analytical stiffness of the portal frames

The measured lateral load–displacement curve for the C20018 frame is presented in Fig. 7(a). The results obtained from frame response modelling (according to Sections 2.4.4 and 3.1) are also included as follows: rigid joint assumption (denoted ‘Rigid’), upper bound linear joint stiffness (denoted ‘EC3’), and lower bound linear joint stiffness (denoted ‘Zad’). Equivalent experimental and numerical results for the remaining C25020 and C30025 frames are shown in Fig. 7(b) (c),

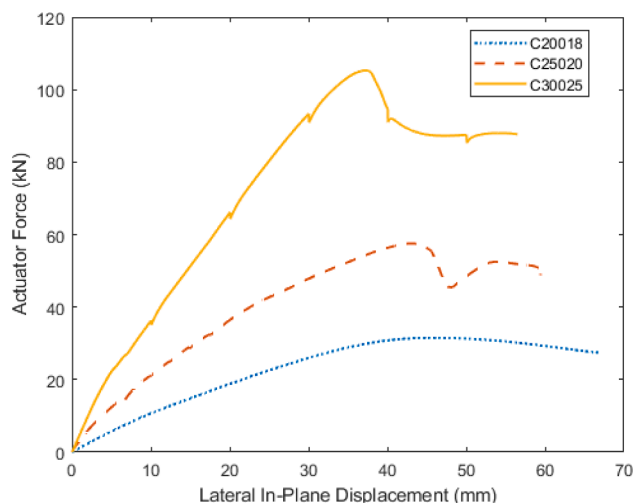


Fig. 6. Experimental load–displacement curves for C20018 (low strength), C25020 (medium strength) and C30025 (high strength) frames.

respectively.

Each of the load–displacement curves demonstrates that the measured lateral force–displacement response of the CFS portal frames agrees with a rigid joint–beam model only at the initial stage of loading. The load–displacement curves start diverging at horizontal loads of approximately 5kN, in all cases. Below this load, friction between plates due to the clamping force from bolts prevents any movement in the joints.

Generally, beam element models using the EC3 joint stiffness values offered conservative predictions of in-service frame deflections, with the numerical curve plotting as a secant to the nonlinear experimental curve. However, for the high strength C30025 frame, the EC3 model predicts an unconservative joint stiffness. The Zad stiffness model leads to conservative frame stiffness predictions for all three frames. As can be seen in Fig. 7, each of the frames retains lateral stiffness after the peak load is reached, and the frames exhibit a mostly ductile post-peak behaviour. In contrast, the lateral response of the frame using a simple beam model is linear and does not capture any nonlinear behaviour, nor the failure load, but the lateral displacement can be quickly estimated without the necessity of employing complex models.

It should be also highlighted that numerically estimated horizontal deflection of tested frames was derived based on the assumption that two channel sections form a compound, doubly symmetric cross-section that is subject to 2-dimensional forces of axial load, shear and major axis bending. The influence of the local buckling, geometrical imperfections or possibility of built-up members acting separately on the members’ flexural stiffness were excluded from the analysis as these factors would not be normally considered in practice. However, as discussed elsewhere in this paper, the above assumptions may need to be adjusted so the deformation of the CFS members is not underestimated.

3.5. Strain gauge results and effect of bi-moment

The longitudinal stresses in the column members were continuously monitored during the tests to evaluate the effect of the bi-moment on frame response. Strain gauges were placed close to the column/bracket junction, on the tension side column of the portal frame so the readings are not distorted by a sudden local buckling of the column. The strain gauges were located at heights of 1315 mm, 1190 mm and 1064 mm from the top of the base plate in the C20018, C25030 and C30025 frames, respectively. A total of six strain gauges were placed in each lipped channel cross-section, located 10 mm from each corner as shown in Fig. 8.

The measured strains were converted to equivalent elastic stresses for three load levels: approximately 30 %, 70 %, and 100 % of the peak lateral load, F_{max} . The 30 % ($0.3F_{max}$) and 70 % ($0.7F_{max}$) values represent the elastic range and the approximate unfactored design load, respectively. These measured values are compared to analytical stresses at each strain gauge location due to the internal forces in a single channel section. This analysis is based on the assumption that in the back-to-back section, the two separate channels share the load equally but each act as an independent member.

3.6. Analytical and experimental stress

Longitudinal stresses were calculated at each strain gauge location, SG1 to SG6 (refer to Fig. 8) using the CUFSM v.4 open-source software [54]. The individual stress components due to uniform tension, major axis bending, minor axis bending and bi-moment are obtained separately along with the total superimposed stress distribution. The magnitudes of the uniform tension, major axis and minor axis bending moment were directly obtained from frame beam analysis model as described in Section 3.1. It should be noted that empirical rotational stiffnesses of column bases were also modelled (C20018 – 52 kNm/rad, C25020 and C30025 – 68 kNm/rad). The bi-moment was calculated using formula presented by Dubina et al., [35], following a procedure as

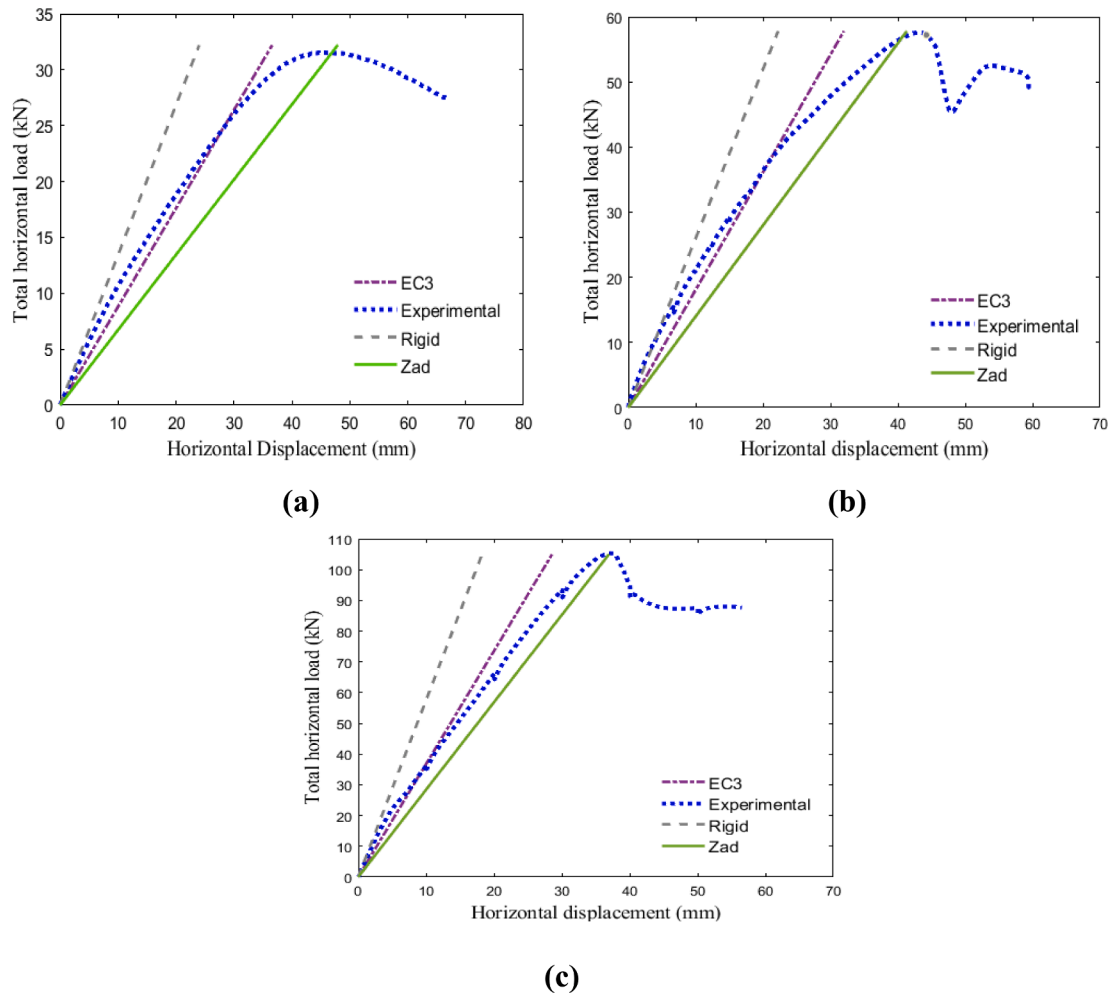


Fig. 7. Load-displacement curves for; (a) C20018; (b) C25020; and (c) C30025 frame.

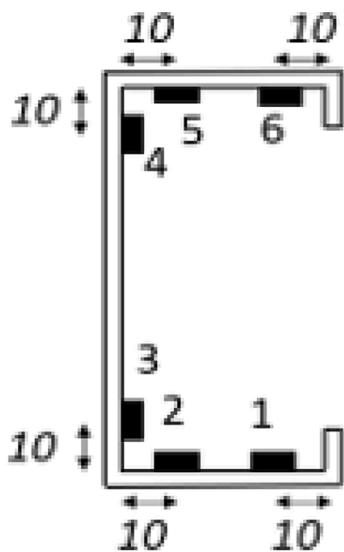


Fig. 8. Location of strain gauges in column cross-section [43].

described by McCrum et al., [43].

The comparison of experimental and analytical stress distributions at the elastic ($0.3F_{max}$), design ($0.7F_{max}$) and the peak (F_{max}) lateral load is presented in Tables 5–7, respectively for the C25020 frame.

3.7. Discussion of results

A consistent pattern of behaviour was observed across all three test frames. At 30 % of the peak load, the material response is in the elastic range and local buckling did not occur in the columns. Hence, all the test frames exhibit a relatively good agreement between the measured and the calculated stresses but only in the web and flange/web junctions (Refer to Column [7] for SG2 and SG5 in Tables 5 to 7). The bi-moment stresses generated a stress concentration at the web/flange junction (location SG3 – see Fig. 8 for SG locations) in all sections. The longitudinal compressive stresses due to bi-moment at SG3 location represent 40.1 %, 38.0 % and 39.3 % of the total stress in the C20018, C25020 and C30025 frames, respectively. This is the second largest contribution to total stress after that due to major axis bending. The calculated averaged ratio of bi-moment to total stress in C20018, C25020 and C30025 sections for varying lateral loads is presented in Table 9. The recorded stress gradients in both flanges also demonstrated that back-to-back channels do not act as doubly symmetric sections. Significantly, the least accurate of the calculated stresses was observed for flange/lip junctions (see locations SG1 – compression and SG6 – tension). In the case of frame C30025, tensile stresses were underestimated by 191.0 % (see Table 8). This was the highest under-conservative prediction of stresses in all 3 frames.

At 70 % of the peak lateral load, a similar trend was observed and stresses in the webs (SG3 and SG4) were generally overestimated between 13.8 % and 35.0 % for C30025 and C20018 frames, respectively (see Table 8). In the case of stresses at flange/lip junctions, the

Table 5
Calculated stresses in a single C25020 section for a lateral load of $F = 17.43 \text{ kN}$ ($0.3F_{\max}$).

Strain gauge	Stresses (MPa)						Percentage Difference (%) [7]	Percentage of Bi-moment w.r.t. Total Stress (%) [8]
	Uniform Tension (N = 5.27 kN) [1]	Major Axis Bending ($M_y = 4.95 \text{ kNm}$) [2]	Minor Axis Bending ($M_z = 0.098 \text{ kNm}$) [3]	Bi-moment ($B_w = 0.079 \text{ kN m}^2$) [4]	Summation of Analytical Stresses (MPa) [5]	Test Results [6]		
SG1	6.3	-78.5	-7.3	43.3	-36.1	-60.9	-68.5	119.9
SG2	6.3	-78.5	1.2	-27.3	-98.3	-83.2	15.4	27.8
SG3	6.3	-71.7	3.0	-38.3	-100.7	-80.9	19.7	38.0
SG4	6.3	71.7	3.0	38.3	119.3	98.5	17.4	32.1
SG5	6.3	78.5	1.2	27.3	113.3	99.1	12.5	24.1
SG6	6.3	78.5	-7.3	-43.3	34.1	55.4	-62.4	127.0
						Avg.	-11.0	61.5

$$1. [7] = \left(\frac{[5] - [6]}{[5]} \right) * 100\%$$

$$2. [8] = \left| \frac{[4]}{[5]} \right| * 100\%$$

3. Sign convention for stress: Positive (+) stress indicates tensile stress, negative (-) stress indicates compressive stress.

4. Sign convention for percentage difference: Positive (+) – stress overestimated in the analytical method, negative (-) – stress underestimated in the analytical method.

Table 6
Calculated stresses in a single C25020 section for a lateral load of $F = 40.65 \text{ kN}$ ($0.7F_{\max}$).

Strain gauge	Stresses (MPa)						Percentage Difference (%) [7]	Percentage of Bi-moment w.r.t. Total Stress (%) [8]
	Uniform Tension (N = 12.29 kN) [1]	Major Axis Bending ($M_y = 11.55 \text{ kNm}$) [2]	Minor Axis Bending ($M_z = 0.228 \text{ kNm}$) [3]	Bi-moment ($B_w = 0.185 \text{ kN m}^2$) [4]	Summation of Analytical Stresses [5]	Test Results [6]		
SG1	14.6	-183.0	-17.0	101.1	-84.3	-147.8	-75.4	119.9
SG2	14.6	-183.0	2.9	-63.8	-229.3	-181.7	20.8	27.8
SG3	14.6	-167.2	7.1	-89.4	-234.9	-173.3	26.2	38.0
SG4	14.6	167.2	7.1	89.4	278.2	241.7	13.1	32.1
SG5	14.6	183.0	2.9	63.8	264.3	251.2	5.0	24.1
SG6	14.6	183.0	-17.0	-101.1	79.6	107.5	-35.1	127.0
						Avg.	-7.6	61.5

Table 7
Calculated stresses in a single C25020 section for a lateral load of $F = 57.3 \text{ kN}$ (F_{\max}).

Strain gauge	Stresses (MPa)						Percentage Difference (%) [7]	Percentage of Bi-moment w.r.t. Total Stress (%) [8]
	Uniform Tension (N = 17.32 kN) [1]	Major Axis Bending ($M_y = 16.28 \text{ kNm}$) [2]	Minor Axis Bending ($M_z = 0.321 \text{ kNm}$) [3]	Bi-moment ($B_w = 0.263 \text{ kN m}^2$) [4]	Summation of Analytical Stresses [5]	Test Results [6]		
SG1	20.6	-258.0	-23.9	142.5	-118.8	-193.0	-62.4	119.9
SG2	20.6	-258.0	4.1	-89.9	-323.2	-238.1	26.3	27.8
SG3	20.6	-235.7	10.0	-126.0	-331.1	-223.9	32.4	38.0
SG4	20.6	235.7	10.0	126.0	392.2	425.7	-8.5	32.1
SG5	20.6	258.0	4.1	89.9	372.6	428.0	-14.9	24.1
SG6	20.6	258.0	-23.9	-142.5	112.2	104.4	7.0	127.0
						Avg.	-3.4	61.5

magnitudes of the tensile stresses (SG6) in frames C20018 and C30025 were underestimated by 17.9 % and 98.6 %, respectively (see Table 8). In the case of frame C25020, the stress in the flange/lip junction in compression was also underestimated by 75.4 % (SG1) (refer to Table 8).

The effect of local buckling on the strain gauge readings and load redistribution would be expected to be the largest at the peak lateral load, hence the largest differences can be expected in this loading scenario. The outermost corner regions (SG1 and SG6) were the most affected in all three frames, and the under-conservative prediction ranged between 26.6 % and 62.4 % (see Table 8). Better agreement between the experimental and analytical results was observed at the web/flange junction. The following percentage differences were recorded at location SG4: 23.3 %, -8.5 % and 6.9 % for the C20018, C25020 and C30025 frames, respectively. The maximum safe (+ve) and

maximum unsafe (-ve) percentage differences (considering all the strain gauge locations, SG1 to SG6) between the measured and analytical stresses in all the three test frames at 30 %, 70 % and 100 % of the peak lateral load are summaries in Table 8.

4. Resistance of lipped channel sections considering monosymmetric and doubly symmetric conditions

The resistance of the tested frames was assessed according to existing design analysis methods. It is possible to calculate the design resistance of the frame members as either a pair of monosymmetric channel sections in a back-to-back arrangement or as a single doubly symmetric back-to-back channel section. In either case, the resistance of the member cross-section, when subjected to the combined effect of

Table 8
Comparison of average measured and experimental stresses.

Frame	Percentage difference between analytical and experimental stresses (%)		
	Maximum under-conservative (–) [SG #]	Maximum conservative (+) [SG #]	Average of all strain gauges
Lateral Load – 0.3 F_{max}			
C20018	–32.7 [#6]	23.0 [#3]	1.6
C25020	–68.5 [#1]	19.7 [#3]	–11.0
C30025	–191.0 [#6]	6.8 [#3]	–47.6
Lateral Load – 0.7 F_{max}			
C20018	–17.9 [#6]	35.0 [#4]	17.9
C25020	–75.4 [#1]	26.2 [#3]	–7.6
C30025	–98.6 [#6]	13.8 [#3]	–26.9
Lateral Load – F_{max}			
C20018	–26.6 [#6]	48.2 [#1]	14.5
C25020	–62.4 [#1]	32.4 [#3]	–3.4
C30025	–47.3 [#1]	32.8 [#3]	–0.7

Table 9
Calculated averaged ratio (of all strain gauge locations SG1 to SG6) of bi-moment to total stress in C20018, C25020 and C30025 section for varying lateral loads.

Frame	Ratio of bi-moment w.r.t. Total Stress for 0.3F _{max} (%)	Ratio of bi-moment w.r.t. Total Stress for 0.7F _{max} (%)	Ratio of bi-moment w.r.t. Total Stress for F _{max} (%)
C20018	59.8	59.8	59.8
C25020	61.5	61.5	61.5
C30025	77.9	77.9	77.9
Average	66.4	66.4	66.4

compression and bending, can be verified in accordance with Equation 6.25, clause 6.19 of EN 1993–1-3:2006 [33] (Eq. (1)):

$$\frac{N_{Ed}}{N_{c,Rd}} + \frac{M_{y,Ed} + \Delta M_{y,Ed}}{M_{cy,Rd,com}} + \frac{M_{z,Ed} + \Delta M_{z,Ed}}{M_{cz,Rd,com}} \leq \quad (1)$$

Similarly, the buckling resistance of the cross-section can be checked using two interaction equations as per clause 6.3.3 (4) of EN-1993-1-1: (2005) [34]:

$$\frac{N_{Ed}}{\chi_y N_{c,Rd}} + k_{yy} \frac{M_{y,Ed} + \Delta M_{y,Ed}}{\chi_{LT} M_{cy,Rd,com}} + k_{yz} \frac{M_{z,Ed} + \Delta M_{z,Ed}}{M_{cz,Rd,com}} \leq 1.0 \quad (2)$$

$$\frac{N_{Ed}}{\chi_z N_{c,Rd}} + k_{zy} \frac{M_{y,Ed} + \Delta M_{y,Ed}}{\chi_{LT} M_{cy,Rd,com}} + k_{zz} \frac{M_{z,Ed} + \Delta M_{z,Ed}}{M_{cz,Rd,com}} \leq 1.0 \quad (3)$$

where;

N_{Ed}	=	Axial compression force
$M_{y,Ed}$	=	Bending moment about the major (y-y) axis.
$M_{z,Ed}$	=	Bending moment about the minor (z-z) axis.
$\Delta M_{y,Ed}, \Delta M_{z,Ed}$	=	Additional moments due to the shift of the centroidal axis for class 4 sections.
$N_{c,Rd}$	=	Design resistance of the cross-section in axial compression (class 4).
$M_{cy,Rd,com}$	=	Design resistance of the cross-section for maximum compressive stress when subjected to bending moment about y-y axis only (class 4).
$M_{cz,Rd,com}$	=	Design resistance of the cross-section for maximum compressive stress when subjected to bending moment about z-z axis only (class 4).
χ_y, χ_z	=	Reduction factor for flexural buckling
χ_{LT}	=	Reduction factor for lateral torsional buckling
$k_{yy}, k_{yz}, k_{zy}, k_{zz}$	=	Interaction factors from EN-1993-1-1:(2005) [34]

In the doubly symmetric condition, because of the geometric symmetry, the eccentricity of the neutral axis of the effective section, with respect to that of the gross cross-section is zero. Hence, the additional moment components in (Eq. (2)) & (Eq. (3)), $\Delta M_{y,Ed}$ and $\Delta M_{z,Ed}$, do not exist. Due to the cross-section being doubly symmetric, the load is applied through the shear centre hence the warping torsion does not need to be considered. However, these bending moment components and bi-moment do exist in the monosymmetric case. Additionally, the eccentricity between the centroid of the single channel and the point of application of the load causes a moment (M_x) about the minor axis.

The lateral torsional buckling capacity of the column members can be determined according to EN-1993-1-3 [33], Clause 6.2.4 and EN-1993-1-1 [34], Clause 6.3.2.2. In this context, Trahair et al., [31] and Woolcock et al., [32] acknowledge that Eurocodes [33–34] consider the monosymmetric beam to be the same as the doubly symmetric beam when calculating the elastic critical moment for lateral torsional buckling. This consideration may lead to unsafe results in some cases. Trahair et al., [31] characterise the asymmetry property of the cross-section about the major y-y axis, by a parameter β_y . If the section is symmetric about the major (y-y) axis, then β_y is equal to zero and the elastic critical moments M_{cr} of the monosymmetric and doubly symmetric section have the same value. However, little design guidance is provided in the literature to account for the asymmetry of the section about the minor (z-z) axis.

As per the design scenarios described above, three different design cases are investigated by comparing the design resistances of the test frame members with the maximum forces experienced during the monotonic tests. The design cases considered are:

Case I: Design as a doubly symmetric section as per [35]

Case II: Design as a monosymmetric section subject to combined major axis bending and bi-moment (B_w), considering the asymmetry parameter, $\beta_y = 0$.

Case III: Design as monosymmetric section subject to combined major axis bending and bi-moment (B_w), considering asymmetry of the section about the minor (z-z) axis ($\beta_y > 0$). In this case, β_y has been considered as the distance between the shear centre and centre of gravity, about the minor axis.

The Eurocode 3 [33,34] resistance checks were carried out considering the effects of combined actions at the critical section at the column and bracket junction, for the ultimate load measured in each test (F_{max}). These internal forces at the critical section of the right-hand side column (refer to Fig. 4) were obtained using the beam element model with semi-rigid joints described in Sections 2.4.4 and 3.1 and are presented in Table 10. The effective length (l_{eff}) of the columns is taken as the distance between the baseplate and the compressed column-bracket junction (see Table 10).

The effective section properties of tested channels were calculated using EN 1993-1-3:2006 [33] for axial compression, bending about y and z-axis and are presented in Table 11. It should be noted that the simplified design procedure presented in Section 5.5.3 of Eurocode 3 [33] is suitable for deriving the effective width and effective thickness of individual plates subject to major axis bending stresses. The effect of the combined action of moment and bi-moment and the extra compression in the web due to bi-moment was expressed via an equivalent reduced effective section under major axis bending ($W_{eff,y+Bw,com}$). It was not possible to implement the combined stresses for these two actions into the simplified design method (Section 5.5.3 of [33]), therefore Finite Strip Software CUFSM v.4.03 [54] was used and the elastic buckling stresses were established using this more advanced numerical tool.

Fig. 9 shows a difference between the longitudinal stresses resulting from major axis bending (simplified design method [33]) and combined bending and bi-moment stresses (using a superposition) as entered in the CUFSM v.4.03 software. The magnitudes of the applied actions and the respective longitudinal stresses are presented in Table 7 columns [1] to

Table 10
Actions calculated for tested frames at the peak experimental loads.

Section	Design Case	l_{eff} (mm)	F_{max} (kN)	N_{Ed} (kN)	$M_{y,Ed}$ (kNm)	$B_{w,Ed}$ (kNm ²)	$M_{z,Ed}$ (kNm)
2xC20018	I	1425	31.60	19.08	21.40	–	–
C20018	II		15.80	9.54	10.70	0.177	0.202
C20018	III		15.80	9.54	10.70	0.177	0.202
2xC25020	I	1301	57.60	35.30	36.11	–	–
C25020	II		28.80	17.65	18.06	0.274	0.327
C25020	III		28.80	17.65	18.06	0.274	0.327
2xC30025	I	1174	105.30	64.90	51.49	–	–
C30025	II		52.65	32.45	30.24	0.551	0.737
C30025	III		52.65	32.45	30.24	0.551	0.737

Table 11
Effective section properties calculated according to Eurocode 3 for sections class 4 [33]

Section	Design Case	$A_{eff,c}$ (mm ²)	$W_{eff,y,com}$ (mm ³)	$W_{eff,y+Bw,com}$ (mm ³)	$W_{eff,z,com}$ (mm ³)
C20018	I	685.5	60797.5	–	–
	II	342.8	–	27388.9	8293.0
	III	342.8	–	27388.9	8293.0
C25020	I	791.6	87959.0	–	–
	II	395.8	–	38058.8	9260.4
	III	395.8	–	38058.8	9260.4
C30025	I	1170.7	154479.6	–	–
	II	585.3	–	70962.1	16471.2
	III	585.3	–	70962.1	16471.2

[4]. The results of these analyses are presented in Fig. 10 for all three tested sections. The other alternative methods for deriving the elastic buckling stresses are the non-linear Finite Element Method (FEM) or buckling tests, which both require significantly more effort (time and resources).

It should be highlighted that the critical buckling stresses for the local buckling were easily established but the distortional buckling minima were less evident for all three sections. It was therefore assumed that the local buckling stresses ($\sigma_{eq,cr,l}$) will be used as a limiting value for calculating effective width and effective thickness for lower bound

resistance. Using the standard method and the limiting value of the buckling stress, the equivalent effective modules for minor axis bending, incorporating the effect of bi-moment ($W_{eff,y+Bw,com}$), was derived and is presented in Table 11. The resistance checks obtained by applying Eqs. (1)–(3) to each of the three design cases for the ultimate load obtained from the testing are presented in Table 12.

The calculated resistance ratios presented in Table 12 range from 0.831 to 1.321. Values of the resistance ratios greater than 1.0 are on the safe side as the actual strength is underestimated. When a doubly symmetric cross-section (Case I) is assumed, the majority of resistance ratios are less than 1.0, implying that this assumption overestimated the strength in two out of three tests. The interaction ratios calculated assuming a monosymmetric cross-section (Cases II and III) are higher than observed for Case I. This applies to both cross-section (Eq. (1)) and member (Eqs. (2) and (3)) level analyses. In Cases II and III (Eq. (1)) where the effect of bi-moment is considered, the experimentally-observed local buckling failure is successfully predicted in two out of the three test frames. It should be also noted that in the case of the smallest section, the local resistance check is short of unity by 1.6 % (Eq. (1)) representing a minor unsafe estimation. When the asymmetry of the cross-section about the minor axis is taken into account, the resistance ratios for combined effects of flexural and torsional buckling further increase in Case III compared to Case II. In every case, the interaction equations are more conservative for global failure than for member local buckling check, which contrasts with the form of experimentally-observed failure in all three tests.

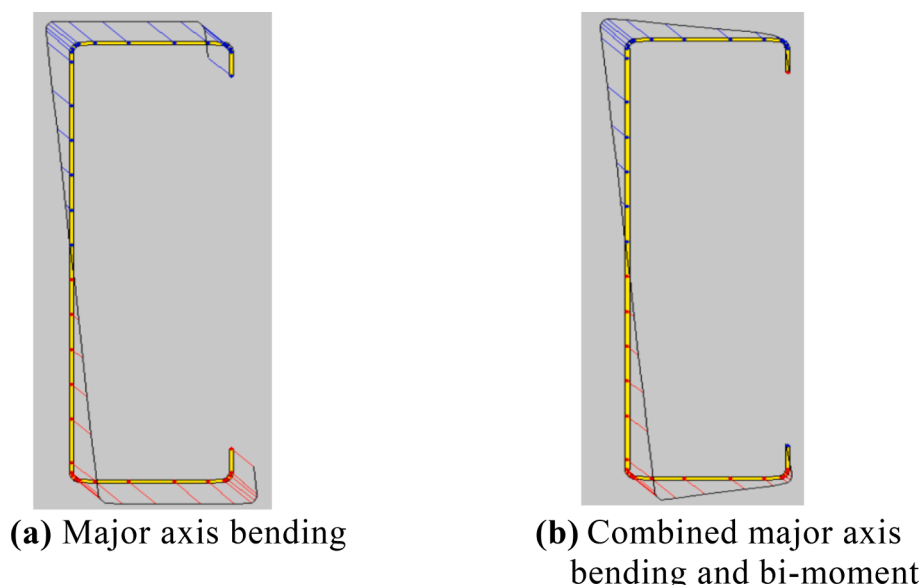


Fig. 9. Input stresses diagrams for C25020 section as modelled in CUFSM v.4.03 [54].

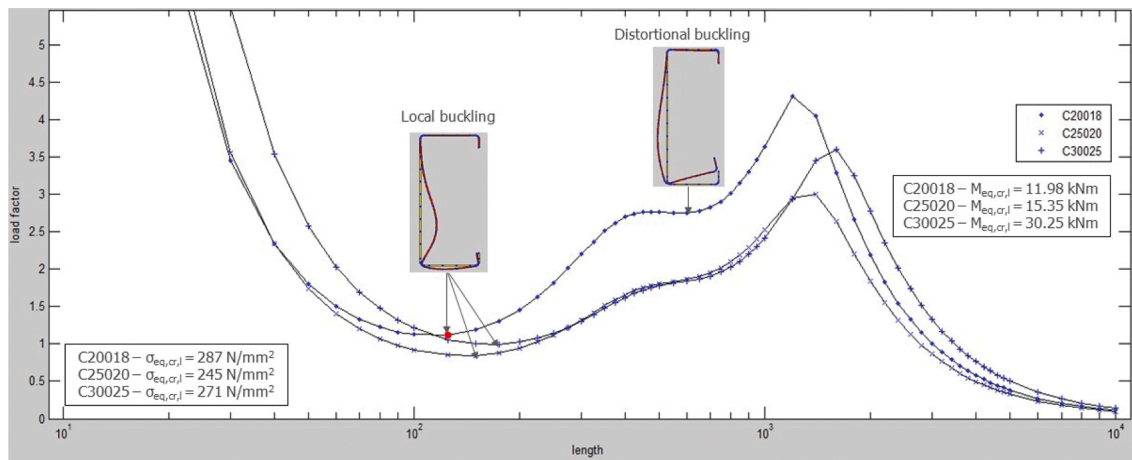


Fig. 10. Signature curves for C20018, C25020, and C30025 sections loaded with combined bending ($M_{y,Ed}$) and bi-moment ($B_{w,Ed}$) stresses obtained from CUFSM v.4.03 based on [54].

Table 12
Resistance checks of lipped channel column members considering design Cases I, II and III.

Section	Design Case	Resistance check (Eq. (1))	Resistance check (Eq. (2))	Resistance check (Eq. (3))
C20018	I	0.831	0.889	0.893
	II	0.984	1.070	1.078
	III	0.984	1.128	1.135
C25020	I	0.944	1.005	1.011
	II	1.182	1.272	1.281
	III	1.182	1.312	1.321
C30025	I	0.941	0.966	0.969
	II	1.120	1.161	1.168
	III	1.120	1.186	1.192

1. Ratios below 1 represent unsafe resistance predictions.
2. Critical resistance checks are highlighted in bold.

5. Conclusions

An experimental and analytical investigation of the behaviour of CFS moment-resisting frames with prototypes of zero-tolerance joints subjected to monotonic lateral loading has been presented. Experimental and analytical lateral load–deflection plots for full-scale frame tests were observed to correlate well with each other when the semi-rigid stiffness of the joint is considered in the analysis. The stiffness model proposed by Zadanfarrokh [36] predicted conservative bearing stiffness of zero-tolerance bolts (shear plane passing through the thread), while the Eurocode 3 model predicted connection stiffness more accurately for the low (C20018) and medium (C25020) strength test frames. It should be noted that lateral deformations in all 3 tested frames were derived based on the assumption that members are doubly symmetric (Case 1) and this design case was shown to produce unconservative strength predictions. Further research should therefore investigate the influence of the combined bending and bi-moment on the frame deformation and how this problem can be implemented in the current design practice.

The ultimate resistance of the column members in the moment-resisting frames were more reliably evaluated when design analysis considered them as monosymmetric cross-sections with the inclusion of extra longitudinal stresses resulting from the bi-moment. Assuming that the back-to-back channels can be designed as doubly symmetric sections, led to an under-conservative assessment of the ultimate resistances of test frames.

The results presented in this paper confirm the feasibility of medium-

span moment-resisting CFS frame structures using zero-tolerance bolted connections while identifying the need to accurately evaluate frame stiffness, longitudinal column stresses and ultimate resistance under combined axial force, biaxial bending and bi-moment.

Declaration of Competing Interest

The authors declare that they have no known competing financial interests or personal relationships that could have appeared to influence the work reported in this paper.

Acknowledgement

This research is funded by a School of Civil Engineering, University College Dublin PhD Scholarship and by an Institution of Civil Engineers, Research & Development Grant (No.1314). The in-kind support from the Capital Steel Buildings and A Steadman & Son should be greatly acknowledged. Technical staff in the Structural Engineering Laboratory in Trinity College Dublin contributed to the completion of the full-scale experiments on CFS test frames.

References

- [1] Target Zero, Guidance on the design and construction of sustainable, low carbon warehouse buildings. 2011, Tata Steel and the British Constructional Steelwork Association. p. 6.
- [2] Roy K, Mohamadjani C, Lim JB. Experimental and numerical investigation into the behaviour of face-to-face built-up cold-formed steel channel sections under compression. *Thin-Walled Struct* 2019;134:291–309.
- [3] Roy K, Ting TCH, Lau HH, Lim JBP. Experimental and numerical investigations on the axial capacity of cold-formed steel built-up box sections. *J Constr Steel Res* 2019;160:411–27.
- [4] Roy K, Lau HH, Ting TCH, Chen B, Lim JBP. Flexural capacity of gapped built-up cold-formed steel channel sections including web stiffeners. *J Constr Steel Res* 2020;172:106154.
- [5] Georgieva I, Schueremans L, Pyl L. Composed columns from cold-formed steel Z-profiles: Experiments and code-based predictions of the overall compression capacity. *Eng Struct* 2012;37:125–34.
- [6] Phan DT, Lim JB, Tanyimboh TT, Sha W. Optimum design of cold-formed steel portal frame buildings including joint effects and secondary members. *Int J Steel Struct* 2017;17(2):427–42.
- [7] Baigent AH, Hancock GJ. The strength of cold-formed portal frames. In: 6th International Specialty Conference in Cold-Formed Steel Structures. Missouri, USA: St Louis; 1982. p. 321–47.
- [8] Kirk P. Design of a cold formed section portal frame building system. In: 8th International Specialty Conference on Cold-Formed Steel Structures. Missouri, USA: St. Louis; 1986. p. 295–310.
- [9] Rensburg BWJ, De Vos GP. Lower cost lightweight cold-formed portal frames. In: 13th International Specialty Conference in Cold-Formed Steel Structures. Missouri, USA: St Louis; 1996. p. 373–88.
- [10] Mills S, LaBoube JR. Self-drilling screw joints for cold-formed channel portal frames. *J Struct Eng* 2004;130(11):1799–806.

- [11] Wrzesien AM, Lim JBP, Nethercot DA. Optimum joint detail for a general cold-formed steel portal frame. *Adv Struct Eng* 2012;15(9):1623–39.
- [12] Lim JBP, Nethercot DA. Serviceability design of a cold-formed steel portal frame having semi-rigid joints. *Steel Compos Struct* 2003;3:451–74.
- [13] Lim JBP, Nethercot DA. Ultimate strength of bolted moment-connections between cold-formed steel members. *Thin-Walled Struct* 2003;41:1019–39.
- [14] Lim JBP, Nethercot DA. Stiffness prediction for bolted moment-connections between cold-formed steel members. *J Constr Steel Res* 2004;60(1):85–107.
- [15] Chung, K.F., et al., *Advances in analysis and design of cold-formed steel structures*, in Joint Structural Division Annual Seminar 2005. 2005. p. 67-87.
- [16] Chen X, Blum HB, Roy K, Pouladi P, Uzzaman A, Lim JBP. Cold-formed steel portal frame moment-resisting joints: Behaviour, capacity and design. *J Constr Steel Res* 2021;183:106718.
- [17] Mäkeläinen P, Kankaanpää J. Structural design study on a light-gauge steel portal frame with cold-formed sigma sections. In: 13th International Specialty Conference on Cold-Formed Steel Structures. Missouri, USA: St. Louis; 1996. p. 349–71.
- [18] Dubina D, et al. Monotonic and cyclic performance of joints of cold formed steel portal frames. In: Loughlan J, editor. 4th International Conference on Thin-walled structures. UK: Loughborough; 2004. p. 381–8.
- [19] Rhodes, J. and R. Burns, Development of a portal frame system on the basis of component testing, in 18th International Specialty Conference in Cold-Formed Steel Structures. 2006: Orlando, Florida, USA. p. 367-385.
- [20] Kwon YB, Chung HS, Kim GD. Experiments of cold-formed steel connections and portal frames. *J Struct Eng* 2006;132(4):600–7.
- [21] Öztürk F, Pul S. Experimental and numerical study on a full scale apex connection of cold-formed steel portal frames. *Thin-Walled Struct* 2015;94:79–88.
- [22] Wrzesien AM. Effect of stressed skin action on the behaviour of cold-formed steel portal frames with non-linear flexible joints and top-hat purlins. The University of Strathclyde; 2016. Ph.D. Thesis.
- [23] Zhang X, Rasmussen KJR, Zhang H. Structural modeling of cold-formed steel portal frames. *Structures* 2015;4:58–68.
- [24] Wrzesien AM, Lim JB, Xu Y, MacLeod IA, Lawson RM. Effect of stressed skin action on the behaviour of cold-formed steel portal frames. *Eng Struct* 2015;105:123–36.
- [25] Wrzesien AM, Pouladi P, Lim JBP, Simon J, Brian M, McCrum DP. Effect of bolt holes clearance on the sway deflections of cold-formed steel portal frames, in International Conference on Engineering Research and Practice for Steel Construction 2018 (ICSC2018). Hong Kong: China; 2018.
- [26] Pouladi, P., Ronaldson, J., Clifton, G.C., Ingham, J.M., Wrzesien, A.M. and Lim, J. B., 2019, August. Finite-element assisted design of eaves joint of cold-formed steel portal frames having single channel-sections. In *Structures* (Vol. 20, pp. 452-464). Elsevier.
- [27] Lim JB, Hancock GJ, Clifton GC, Pham CH, Das R. DSM for ultimate strength of bolted moment-connections between cold-formed steel channel members. *J Constr Steel Res* 2016;117:196–203.
- [28] Phan DT, Mojtabaei SM, Hajirasouliha I, Lau TL, Lim JBP. Design and optimization of cold-formed steel sections in bolted moment connections considering bimoment. *J Struct Eng* 2020;146:04020153.
- [29] Mojtabaei SM, Becque J, Hajirasouliha I. Local buckling in cold-formed steel moment-resisting bolted connections: behavior, capacity, and design. *J of Struct Eng* 2020;146:04020167.
- [30] Mojtabaei SM, Becque J, Hajirasouliha I. Behavior and design of cold-formed steel bolted connections subjected to combined actions. *J Struct Eng* 2021;147:04021013.
- [31] Trahair N, Bradford MA. *Behaviour and design of steel structures to AS4100*: Australian. CRC Press; 2017.
- [32] Woolcock ST, Bradford MA, Kitipornchai S. *Design of portal frame buildings*. Australian Steel Institute; 2003.
- [33] BS EN 1993-1-3, Eurocode 3 - Design of steel structures, in Part 1-3: General rules - Supplementary rules for cold-formed members and sheeting. 2006, European Committee for Standardization: Brussels.
- [34] CEN. EN-1993-1-1:2005 – Eurocode 3: Design of Steel Structures, Part 1–1: General rules and rules for buildings. Brussels: European Committee for Standardization; 2005.
- [35] Dubina, D., Ungureanu, V. & Landolfo, R. 2012. *Design of Cold-formed Steel Structures: Eurocode 3: Design of Steel Structures. Part 1-3 Design of cold-formed Steel Structures*, Wiley.
- [36] Zadanfarokh, F. and E.R. Bryan. Testing and design of bolted connections in cold-formed steel sections. in 11th International Specialty Conference on Cold-Formed Steel Structures. 1992. St. Louis, Missouri, USA.
- [37] Zaharia R, Dubina D. Stiffness of joints in bolted connected cold-formed steel trusses. *J Constr Steel Res* 2006;62:240–9.
- [38] Dubina D. Structural analysis and design assisted by testing of cold-formed steel structures. *Thin Walled Struct* 2008;46(7–9):741–64.
- [39] Wuwer, W., J. Zamorowski, and S. Swierczyna, Lap joints stiffness according to Eurocode EC3 and experimental investigations results. *Archives of Civil and Mechanical Engineering*, 2012. 12(1): p. 95-104.
- [40] Bučmýs Ž, Daniūnas A, Jaspert J-P, Demonceau J-F. A component method for cold-formed steel beam-to-column bolted gusset plate joints. *Thin-Walled Struct* 2018; 123:520–7.
- [41] BS EN 1993-1-8, Eurocode 3 - Design of steel structures, in Part 1-8: Design of joints. 2005, European Committee for Standardization: Brussels.
- [42] Wrzesien AM, Roy K, Fang Z, Lim JBP. Tests, modelling and design of cold-formed steel moment resisting joints with bolts in the web and outer flange. *Thin-Walled Struct* 2023;182:110176.
- [43] McCrum DP, Simon J, Grimes M, Broderick BM, Lim JB, Wrzesien AM. Experimental cyclic performance of cold-formed steel bolted moment resisting frames. *Eng Struct* 2019;181:1–14.
- [44] McCrum DP, Simon J, Grimes M, Broderick BM, Wrzesien A, Lim JBP. Hybrid seismic testing of cold-formed steel moment-resisting frames. *Proceedings of the Institution of Civil Engineers-Structures and Buildings* 2020;173(2):88–98.
- [45] BS EN ISO 4017: 2014, Fasteners - Hexagon head screws - Product grades A and B (ISO 4017: 2014). 2014, British Standard Institution: London.
- [46] BS EN 10346:2015, Continuously hot-dip coated steel flat products for cold forming Technical delivery conditions. 2015, European Committee for Standardization: Brussels.
- [47] BS EN 10002-1:2001, Metallic materials - Tensile testing, in Part 1: Method of test at ambient temperature. 2001, European Committee for Standardization: Brussels.
- [48] Simulia Inc. ABAQUS Standard (version 6.7-5), 2008.
- [49] Schafer BW, Peköz T. Computational modeling of cold-formed steel: characterizing geometric imperfections and residual stresses. *J Constr Steel Res* 1998;47(3): 193–210.
- [50] Zhao X, Tootkaboni M, Schafer BW. Development of a laser-based geometric imperfection measurement platform with application to cold-formed steel construction. *Exp Mech* 2015;55(9):1779–90.
- [51] Selvaraj S, Madhavan M. Geometric imperfection measurements and validations on cold-formed steel channels using 3D noncontact laser scanner. *J Struct Eng* 2018; 144(3):04018010.
- [52] Autodesk Inc. Autodesk Robot Structural Analysis Professional 2010 Training Manual - Metric Version. 2009.
- [53] SCI P212, Joints in steel construction: simple connections 2009, The Steel Construction Institute: Ascot, UK.
- [54] Z. Li, B.W. Schafer, Buckling analysis of cold-formed steel members with general boundary conditions using CUFMS: conventional and constrained finite strip methods, Proceedings of the 20th International Specialty Conference in Cold-Formed Steel Structures, St Louis, Missouri, USA, 2010.